Japanese Journal of Applied Physics **REGULAR PAPER**

Adaptive Compensation for Angular Deflection of Beams Carrying Orbital Angular Momentum on Mode Sorting

Hiroki Kishikawa*, Noriyuki Sakashita†, and Nobuo Goto

Department of Optical Science, Graduate School of Science and Technology, Tokushima University, Tokushima 770-8506, Japan

Beams carrying orbital angular momentum (OAM) has attracted attention as a potential candidate to expand the transmission capacity in the optical communication. Mode sorting is an efficient method to demultiplex the OAM multiplexed lightwaves. We have reported the mode sorting performance for OAM beams suffering lateral displacement and angular deflection. It was found that the angular deflection was severe, namely, only 100-μrad deflection deteriorated the performance in terms of crosstalk. Thus, the strict angular alignment would be required in the free-space optical communication using OAM multiplexing. In this paper, we propose an adaptive compensation method based on detection of the angular deflection of beams carrying OAM on mode sorting in order to relax such a strict requirement. Numerical simulation results reveal that the compensation in every 100 μrad effectively suppresses the crosstalk caused by the angular deflection.

1. Introduction

Optical transmission capacity has been increased by multiplexing technologies such as wavelength division multiplexing (WDM), polarization division multiplexing (PDM), and space division multiplexing (SDM) for catching up with the growing demand of the communication traffic.[1)] Orbital angular momentum (OAM) is one of the orthogonal spatial modal basis for mode division multiplexing (MDM) technology.[2)] OAM beams have an advantage that different azimuthal OAM states are mutually orthogonal while propagating coaxially. This orthogonality increases the transmission capacity by using multiple OAM states together with other multiplexing technologies. There are various applications of OAM beams other than optical communication such as optical tweezing,[3,4)] laser material surface processing,[5,6)] quantum entanglement,[7,8)] image processing[9)] and quantum metrology.[10)]

OAM beams are characterized by helical phase front and usually have an annular ring intensity profile with a phase singularity at the beam center. The helical phase front is de-

*E-mail: kishikawa.hiroki@tokushima-u.ac.jp
†H. Kishikawa and N. Sakashita equally contributed to this work

scribed by a phase term of exp($im\phi$) in analytic expression, where ϕ is the rotation angle on the azimuthal coordinate and m is an integer called topological charge (TC) which means the number of intertwined helices. Representative OAM beams are Laguerre-Gaussian (LG) beam[11,12] and Bessel-Gaussian (BG) beam.[13,14] Another OAM beam called 'perfect vortex' (PV) beam is generated by taking the spatial Fourier transform of BG beam.[15] This beam has a unique characteristic that whose ring width and average ring diameter do not strongly depend on TC.

It is necessary to demultiplex the OAM multiplexed beams to retrieve information carried by each of the OAM modes in the receiver. Demultiplexing can be basically performed by the reciprocal way of the multiplexing such as by using spiral phase plates, cylindrical lens mode converters, fiber mode couplers, q-plates, metamaterial-based phase plate, silicon integrated optics, and spatial light modulators (SLMs).[2,16–19] Recently reported mode sorting methods[20–22] spatially separate OAM multiplexed beams in lateral position in ascending order of TCs by using SLMs and Fourier lenses. The principle is based on a log-polar coordinate transformation followed by a phase correction using SLMs and spatial Fourier transform. The advanced methods[21,22] enable high resolution sorting by employing a beam copy function with the coordinate transformation in order to mitigate overlapping between adjacent sorting results of OAM beams with neighboring TCs. Another high resolution mode sorting method utilizes a spiral coordinate transformation to unwrap OAM beams.[23]

Since OAM transmission is mainly through free-space, misalignment of the transmitter and the receiver may affect the performance of retrieving information carried by each of the OAM modes. Studies[24,25] reported the influence of lateral displacement and angular deflection between the transmitting OAM beams and the receiver plane. However, they did not mention the influence on mode sorting performance. Thus, we firstly reported such influence on ordinary resolution and high resolution mode sorting performances for LG and PV beams by numerically verifying the tolerance.[26,27] We have also reported the influence of distance displacement in Microoptics Conference 2018.[28] The important finding of our investigation so far is that the influence of angular deflection is much more severe and would be a major limiting factor for the mode sorting performance since strict angular alignment within $\pm 100\mu$rad is required. Compared to the angular deflection, the lateral displacement was found to be less severe since displacement within ±20 % of the beam diameter was acceptable. Although the alignment of the transmitter and receiver has once been fixed, the transmitted lightwave experiences beam tilt and wandering due to the turbulent atmosphere in free-space communication.[29,30] The resultant received beam is forced to have angular de-

flection and lateral displacement, which needs to be adaptively compensated to improve the signal quality.

Therefore, in this paper, we propose an adaptive compensation method for the angular deflection and numerically investigate the mode sorting performance with or without compensation. Most of adaptive compensation methods reported so far for OAM carrying beam in literature[31–33] aimed to compensate for stochastic amplitude and phase fluctuation due to atmospheric turbulence by using iterative feedback processes. The method we proposed in this paper is simpler and does not need such iterative processes since it aims to compensate for the deterministic angular deflection. Figure 1 explains the definition of lateral angular deflection. It is defined by vertical angular deflection γ and horizontal angular deflection ψ expressing the tilted aperture of the mode sorter with respect to the plane perpendicular to beam axis. Our recent report[34] verified the effectiveness of the proposed adaptive compensation method only for the vertical angular deflection. This paper describes more comprehensive explanation of the compensation principle and clarifies its effectiveness for both of the vertical and the horizontal angular deflections. Numerical simulation results reveal that the adaptive compensation effectively compensates for the influence of angular deflection below an acceptable level of crosstalk which is defined in Section 3 as a performance metric.

The rest of the paper is organized as follows. Section 2 describes the principle of adaptive compensation and analytic expression of LG beam, PV beam, and the angular deflection. Section 3 discusses the numerical calculation conditions and the results measured by crosstalk as a performance metric. Section 4 concludes the paper.

2. Adaptive compensation for angular deflection

The principle of adaptive compensation for angular deflection is based on the spatial Fourier transform. The schematic shown in Fig. 2 consists of an adaptive wavefront compensator and a mode sorter. The transmitted beam includes data-carrying multiple OAM beams and a non-data-carrying pilot beam used for detecting the amount of angular deflection. They are assumed to have the same amount of angular deflection. The pilot beam is in 0-th order OAM mode and has an orthogonal polarization state to the data-carrying OAM beams.

A polarization beam splitter (PBS) in the adaptive wavefront compensator extracts the pilot. The extracted pilot is Fourier transformed by passing through a lens. When the pilot has a certain amount of phase tilt due to the angular deflection, the light spot of the Fourier transformed pilot moves on the lateral position according to the phase tilt. After taking the intensity profile by a camera (Rx1), a PC detects the pilot position and calculates the com-

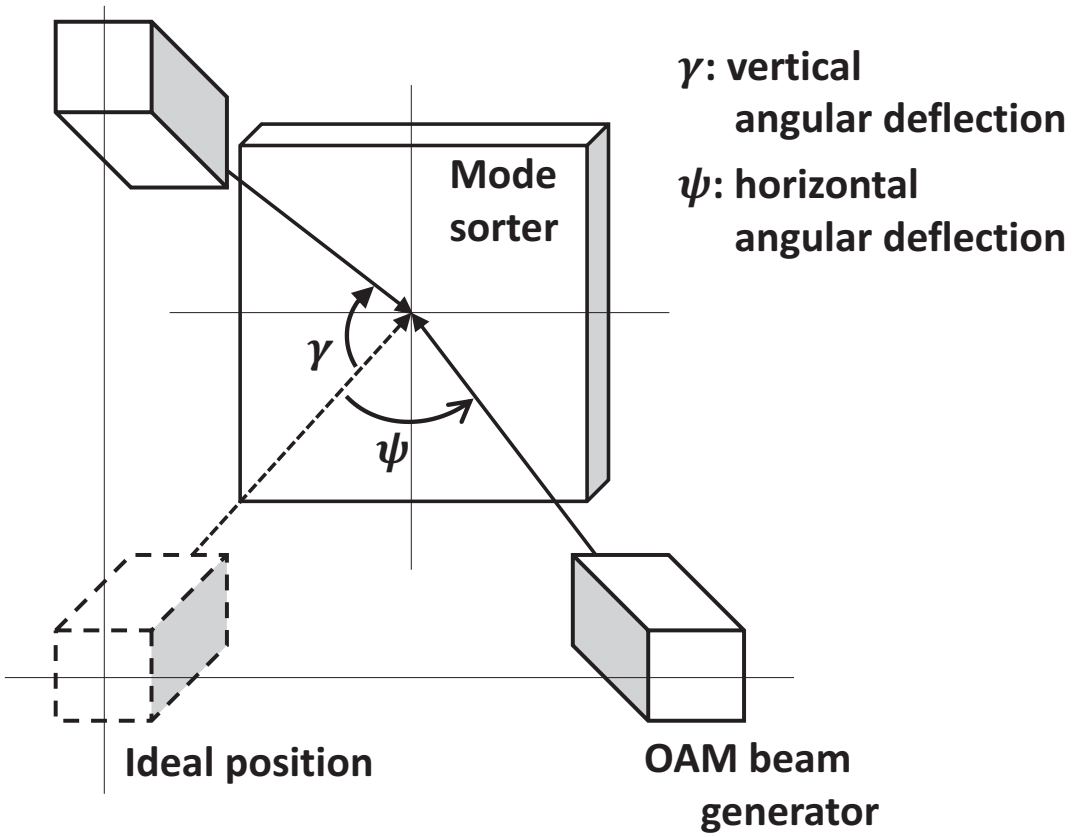

Fig. 1. Lateral displacement and angular deflection.

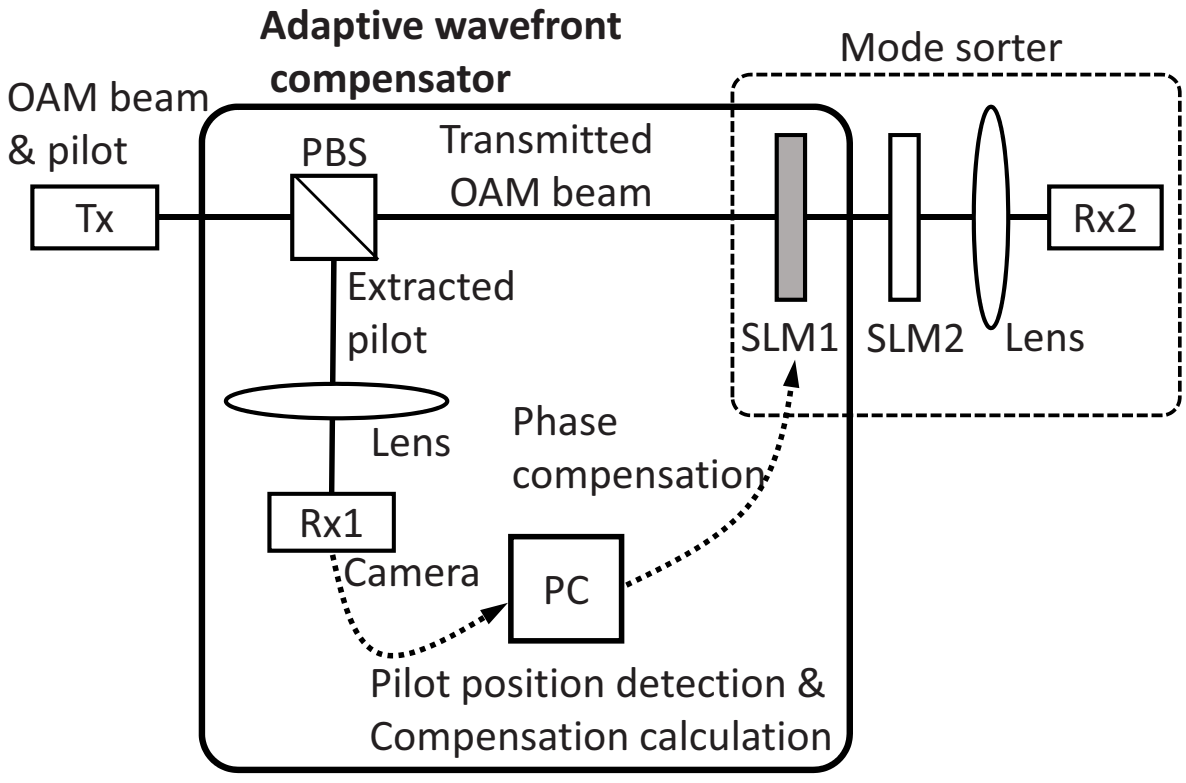

Fig. 2. Schematic of the proposed adaptive compensation method for angular deflection.

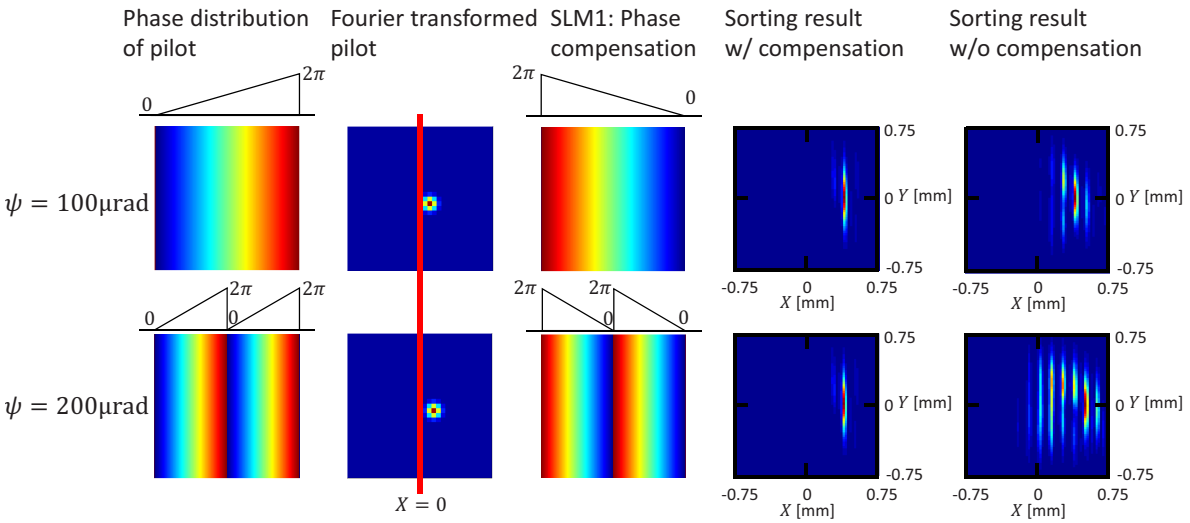

Fig. 3. (Color online) Phase distribution of pilot, intensity profile of pilot after Fourier transform by a lens, compensation phase distribution added to SLM1, sorting results of LG beam ($m = 3$) with and without compensation when horizontal angular deflection $\psi = 100$ and 200μrad.

pensation pattern for the angular deflection based on the detected position. The calculated compensation pattern is the inverse phase tilt of the pilot and is transferred onto the SLM1 in the mode sorter. Thus, the angular deflection on the transmitted data-carrying OAM beams are compensated in the SLM1. Note that the SLM1 displays combined phase distribution not only the compensation pattern but also log-polar coordinate transformation.

Figure 3 shows the phase distribution of the pilot, the intensity profile of the pilot after Fourier transform by a lens, the compensation phase distribution added to SLM1, sorting results of LG beam ($m = 3$) with and without compensation when horizontal angular deflection $\psi = 100$ and 200 μrad. Parameters used in this calculation are summarized in Table I. As shown in the intensity profile of the Fourier transformed pilot, lateral position is moved to right according to the amount of ψ. It is found that the sorting results without compensation are spreading in horizontal direction, which may result in misunderstanding of the included OAM modes in the transmitted beam. This spreading is explained by expanding the tilt term of Eq. (3), namely, exp(·) can be expanded and rearranged with Maclaurin series, power-reduction formulae of the trigonometric function, and Euler's formula. As a result, an LG beam in a tilted coordinate is expressed by the superposition of modes having multiple TCs. Thus, the sorting results without compensation are spreading in horizontal direction. In contrast, the sorting results with compensation have only a single high intensity profile, thus, included OAM modes can be clearly distinguished.

3. Numerical calculation

The mathematical expression of the LG beam with azimuthal index (TC) m and radial index n at waist plane ($z = 0$) is given in cylindrical coordinates (r, ϕ) by

$$LG_{nm}(r,\phi) = \sqrt{\frac{2n!}{\pi w^2 (n+|m|)!}} \left(\frac{\sqrt{2}r}{w}\right)^{|m|} L_n^{|m|}\left(\frac{2r^2}{w^2}\right) \exp\left(-\frac{r^2}{w^2}\right) \exp(im\phi) \tag{1}$$

where $L_n^{|m|}(\cdot)$ is the generalized Laguerre polynomial, $w = w_0\sqrt{1+(z/z_R)^2}$ is the Gaussian radius corresponding to the beam waist of w_0 at $z = 0$, $z_R = \pi w_0^2/\lambda$ is the Rayleigh range, and λ is the wavelength. The ring radius in the intensity profile of the LG beam is related to TC.

The PV beam generated at the focal point of the Fourier lens with focal length f from the BG beam[35] is given by

$$PV_{nm}(r,\phi) = i^{m-1}\frac{w_0}{w} I_m\left(\frac{2rr_0}{w^2}\right) \exp\left(-\frac{r^2+r_0^2}{w^2}\right) \exp(im\phi) \tag{2}$$

where $w = 2f/kw_0$ is the Gaussian radius at the focal point, $I_m(\cdot)$ is an m-th order modified Bessel function of first kind, m corresponds to TC, $r_0 = k_r f/k$ represents the ring radius of the PV beam at the focal point, k_r is the radial wave vector, and $k = 2\pi/\lambda$ is the wave number. When $r = r_0$ and w is small enough, $I_m(\cdot)$ can be approximated to $\exp(\cdot)$. Thus, the beam diameter of the PV beam is not related to TC.

The beam carrying OAM with vertical angular deflection γ and horizontal angular deflection ψ is expressed as[25]

$$OAM_{\mathrm{def}}(r,\phi) = OAM(r,\phi) \exp(ik\tan\gamma \cdot r\sin\phi + ik\tan\psi \cdot r\cos\phi) \tag{3}$$

where function $OAM(r,\phi)$ relates to a beam carrying OAM in an ideal position and free from angular deflection. The proposed adaptive compensation method performs multiplication of the inverse term of $\exp(\cdot)$ in Eq. (3) to the received beam to remove the angular deflection.

Numerical calculations are performed by using Scilab software and the conditions are summarized as Table I. The former five parameters are for the input beams, the following five parameters are for the mode sorter, and the latter two parameters are commonly used. The method of Ref.[22] is used as the high resolution mode sorting for both LG and PV beams. Two copies of the log-polar coordinate transformed beams are placed at both sides of the original transformed beam for the high resolution mode sorter. The reason for the parameter choice is the same as our previous work.[27] Namely, we consider matching of the specifications of equipments we have for future experimental verification and the reproducibility of the reported high-resolution mode sorting method.[22]

Mode numbers included in the received OAM beam can be identified by detecting the

Table I. Numerical calculation conditions.

Parameters	Value
Radial vector index	$n = 0$
Wavelength	$\lambda = 632.8$ nm
LG beam waist	$w_0^{LG} = 1$ mm
PV beam waist	$w_0^{PV} = 0.2$ mm
PV beam radial wave vector	$k_r^{PV} = 40$ mm^{-1}
Size parameter[22)]	$d = 0.1592$ mm
Location parameter[22)]	$p = 0$ mm
Focal length[22)]	$f = 191$ mm
Fan-out optimization parameter[22)]	$a_{\pm1} = -\pi/2, b_{\pm1} = 1.329$
Phase compensation for $-1, 0, +1$-order copies[22)]	$\phi_{bc} = 0, 1.55, 0$
Two dimensional calculation area	6.4×6.4 mm^2
Spatial resolution	25×25 μm^2/pixel

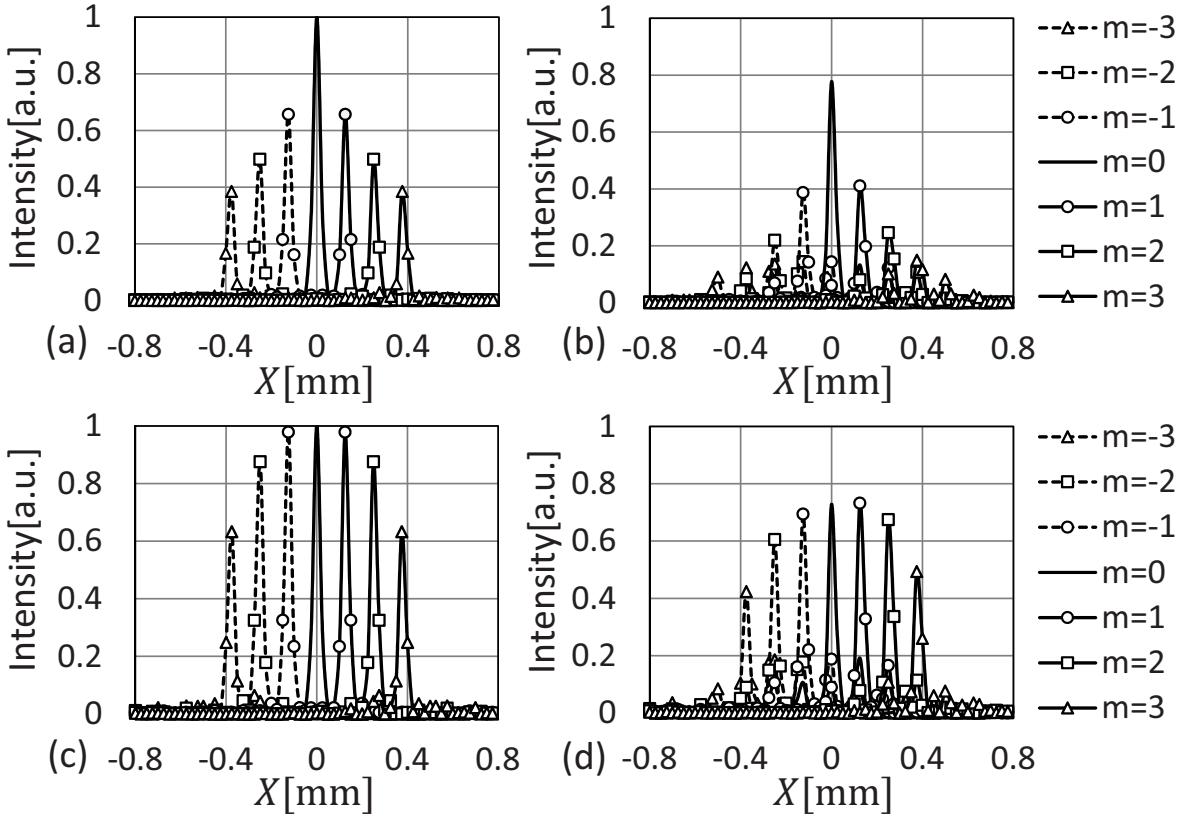

Fig. 4. Intensity profile after mode sorting for (a, b) LG beam and (c, d) PV beam having a single TC of $m = -3, -2, -1, 0, 1, 2, 3$. Panels (a) and (c) are without any angular deflection and panels (b) and (d) are with $\gamma = 100$-μrad vertical angular deflection.

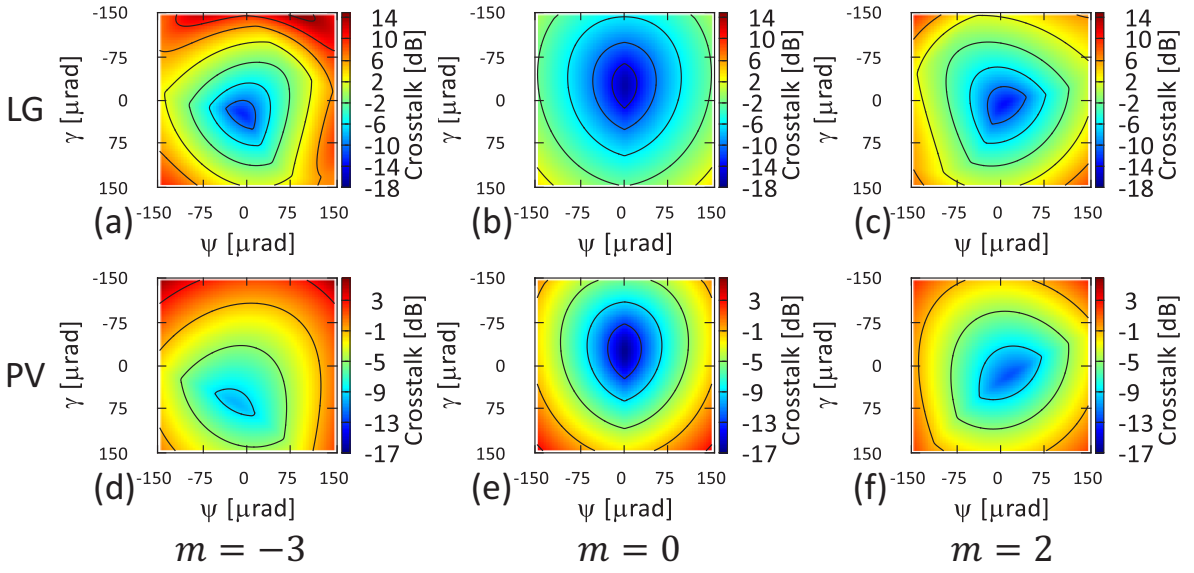

Fig. 5. (Color online) Crosstalk contour maps without compensation as functions of vertical angular deflection γ and horizontal angular deflection ψ for (a, b, c) LG beam and (d, e, f) PV beam. Panels (a) and (d) are $m = -3$, (b) and (e) are $m = 0$, and (c) and (f) are $m = 2$.

intensity profile after mode sorting in the horizontal direction at $Y = 0$ by using, for example, a photo-detector array. Figure 4 shows the intensity profile after mode sorting obtained by such a way on the axis $Y = 0$ for LG beam and PV beam having a single TC of $m = -3, -2, -1, 0, 1, 2, 3$. Figures 4(a) and 4(b) show the intensity profiles without angular deflection and with $\gamma = 100$-μrad vertical angular deflection for LG beam, respectively. Figures 4(c) and 4(d) are those for PV beam. There are small intensity growth by other m in the bottom area at positions corresponding to each of m in Figs. 4(b) and 4(d), which may affect the light intensity detection. Thus, we use crosstalk as a performance metric of the mode sorting. Its definition is the same as our previous study,[27] which is the ratio of the maximum of detected intensities among undesired modes by the intensity of the desired mode as

$$XT_{m=l} = 10 \log_{10} \frac{\max(I_{m \neq l})}{I_{m=l}} \quad [\text{dB}] \tag{4}$$

where l is an integer corresponding to the desired mode and I represents the detected intensity. The detected intensity is calculated by the trapezoidal integration of five consecutive pixels in mode sorting results since it is the maximum number of pixels without overlapping between adjacent modes in our numerical analyses.

Figure 5 shows crosstalk contour maps without compensation as functions of the vertical angular deflection γ and the horizontal angular deflection ψ. Figures 5(a), 5(b), and 5(c) are results for LG beam, and Figs. 5(d), 5(e), and 5(f) are those for PV beam. The transmitted

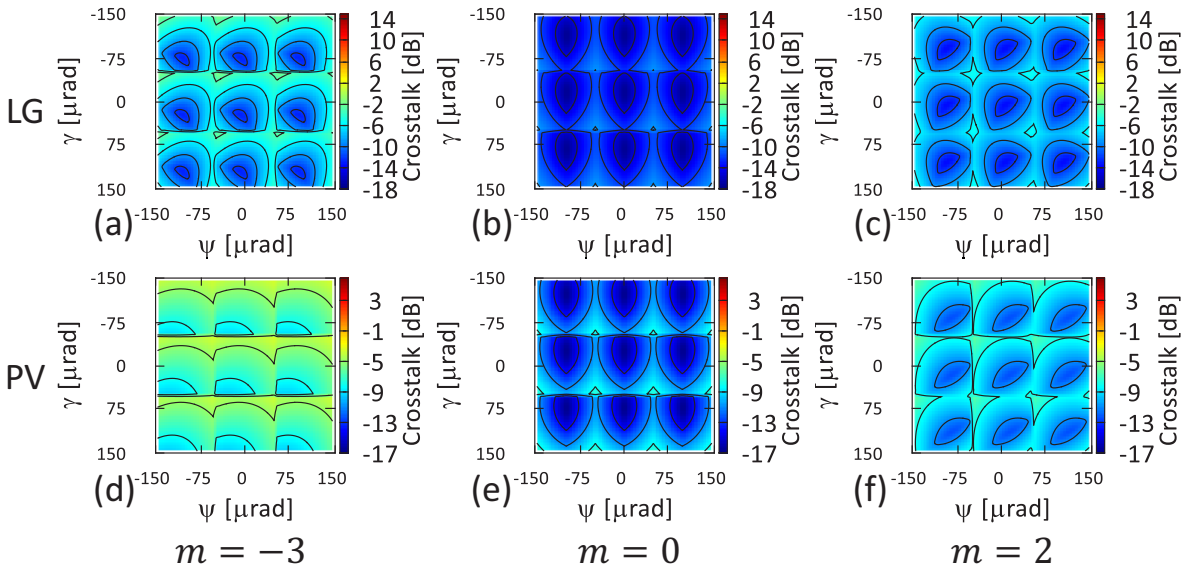

Fig. 6. (Color online) Crosstalk contour maps with compensation as functions of vertical angular deflection γ and horizontal angular deflection ψ for (a, b, c) LG beam and (d, e, f) PV beam. Panels (a) and (d) are $m = -3$, (b) and (e) are $m = 0$, and (c) and (f) are $m = 2$.

LG and PV beams simultaneously include nine TCs of $m = -4, -3, -2, -1, 0, 1, 2, 3, 4$ in this calculation. Between these modes, Figs. 5(a) and 5(d) are $m = -3$, 5(b) and 5(e) are $m = 0$, and 5(c) and 5(f) are $m = 2$. These contour maps have bowl-like shapes with the minimum crosstalk value around zero angular deflection. Focusing on high crosstalk regions, especially four corners of Figs. 5(a), 5(c), 5(d), and 5(f), crosstalk of the LG beam is higher than that of the PV beam. Thus, the LG beam shows weaker tolerance to the angular deflection than the PV beam. This is because the thicker ring width of the intensity profile of LG beam is vulnerable to phase tilt due to the angular deflection in the mode sorting process compared to the thinner ring width of PV beam.

Figure 6 shows crosstalk contour maps with compensation as functions of vertical angular deflection γ and horizontal angular deflection ψ. The panel layout of Fig. 6 is similar to Fig. 5. The only difference is that the adaptive compensation is performed in every 100-μrad angular deflection since it corresponds to one pixel move of the peak intensity on the Fourier plane after the lens in the wavefront compensator with calculation conditions shown in Table I. All contour maps look like 3×3 tiles in which the small crosstalk central square of -50 μrad $\leq \gamma \leq 50$ μrad and -50 μrad $\leq \psi \leq 50$ μrad in Fig. 5 is copied to the surrounded tiles in every 100 μrad. Therefore, the crosstalk is effectively suppressed to be less than -3 dB by the adaptive compensation. Further reduction of crosstalk is achievable by increasing the spatial resolution of the pilot detection and performing compensation in a finer interval of the

angular deflection.

4. Conclusions

We have proposed the adaptive compensation method for angular deflection on OAM mode sorting by detecting the phase tilt of the pilot based on Fourier optics. Numerical calculation for the mode sorting performance revealed that the crosstalk was effectively suppressed by the proposed method. Comparing the performance between LG and PV beams, LG beam provided weaker tolerance to the angular deflection since the thicker ring width of the intensity profile of LG beam was vulnerable to phase tilt in the mode sorting process compared to the thinner ring width of PV beam. Our future works will include experimental verification of the proposed method and consider adaptive compensation methods for lateral displacement. For this purpose, we will also investigate detection methods that recognize the cause of misalignment such as angular deflection, lateral displacement, and both of them.

References

1) P. J. Winzer, Optics & Photonics News, **26**, 28, (2015).
2) A. E. Willner, H. Huang, Y. Yan, Y. Ren, N. Ahmed, G. Xie, C. Bao, L. Li, Y. Cao, Z. Zhao, J. Wang, M. P. J. Lavery, M. Tur, S. Ramachandran, A. F. Molisch, N. Ashrafi, and S. Ashrafi, Advances in Optics and Photonics, **7**, 66, (2015).
3) H. He, M. E. J. Friese, N. R. Heckenberg, and H. Rubinsztein-Dunlop, Phys. Rev. Lett., **75**, 826, (1995).
4) V. Garbin, D. Cojoc, E. Ferrari, R. Z. Proietti, S. Cabrini and E. D. Fabrizio, Jpn. J. Appl. Phys., **44**, 5773, (2005).
5) J. J. J. Nivas, S. He, A. Rubano, A. Vecchione, D. Paparo, L. Marrucci, R. Bruzzese, and S. Amoruso, Sci. Rep., **5**, 17929, (2015).
6) O. J. Allegre, W. Perrie, S. P. Edwardson, G. Dearden, and K. G. Watkins, J. Opt., **14**, 085601, (2012).
7) A. Mair, A. Vaziri, G. Weihs, and A. Zeilinger, Nature, **412**, 313, (2001).
8) A. Vaziri, G. Weihs, and A. Zeilinger, J. Opt. B, **4**, S47, (2002).
9) J. A. Davis, D. E. McNamara, D. M. Cottrell, and J. Campos, Opt. Lett., **25**, 99, (2000).
10) V. D'Ambrosio, N. Spagnolo, L. Del Re, S. Slussarenko, Y. Li, L. C. Kwek, L. Marrucci, S. P. Walborn, L. Aolita, and F. Sciarrino, Nature Commun., **4**, 2432, (2013).
11) L. Allen, M. W. Beijersbergen, R. J. C. Speeruw, and J. P. Woerdman, Phys. Rev. A, **45**, 8185, (1992).
12) M. W. Beijersbergen, L. Allen, H. E. L. O. van der Veen, and J. P. Woerdman, Opt. Commun., **96**, 123, (1993).
13) F. Gori, G. Guattari, and C. Padovani, Opt. Commun., **64**, 491, (1987).
14) J. Durnin and J. J. Miceli Jr., Phys. Rev. Lett., **58**, 1499, (1987).
15) A. Ostrovsk, C. Rickenstor-Parrao, and V. Arrizón, Opt. Lett., **38**, 534, (2013).
16) J. Wang, Proc. Optical Fiber Commun. Conf., 2016, Th1H.5.
17) M. Okamoto and H. Sasada, Jpn. J. Appl. Phys., **44**, 1743, (2005).
18) K. Badham, I. Moreno, M. M. Sánchez-López, J. A. Davis, N. Hashimoto, M. Kurihara, J. Albero, and D. M. Cottrell, Jpn. J. Appl. Phys., **55**, 122202, (2016).
19) R. Kitayama, Jpn. J. Appl. Phys., **52**, 09LD11, (2013).
20) G. C. G. Berkhout, M. P. J. Lavery, J. Courtial, M. W. Beijersbergen, and M. J. Padgett, Phys. Rev. Lett., **105**, 153601, (2010).
21) M. Mirhosseini, M. Malik, Z. Shi, and R.W. Boyd, Nature Commun., **4**[3781], 1, (2013).

22) C. Wan, J. Chen, and Q. Zhan, APL Photon., **2**, 031302, (2017).
23) Y.Wen, I. Chremmos, Y. Chen, J. Zhu, Y. Zhang, and S. Yu, Phs. Rev. Lett., **120**, 193904, (2018).
24) G. Xie, L. Li, Y. Ren, H. Huang, Y. Yan, N. Ahmed, Z Zhao, M. P. J. Lavefy, N. Ashrafi, S. Ashrafi, R. Bock, M. Tur, A. F. Molisch, and A. E. Willner, Optica, **2**, 357, (2015).
25) X. Yin, H. Sang, X. Cui, H. Chang, L. Li, and G. Wu, Opt. Commun., **393**, 34, (2017).
26) N. Sakashita, H. Kishikawa, and N. Goto, Proc. 22nd Microoptics Conf., 2017, P-99.
27) H. Kishikawa, N. Sakashita, and N. Goto, Jpn. J. Appl. Phys., **57**, 08PB01, (2018).
28) N. Sakashita, H. Kishikawa, and N. Goto, Proc. 23nd Microoptics Conf., 2018, P-01.
29) S. Fu and C. Gao, Photonics Research, **5**, B1, (2016).
30) M. Hulea, Z. Ghassemlooy, S. Rajbhandari, and X. Tang, J. Lightw. Technol., **7**, 1323, (2014).
31) Y. Ren, G. Xie, H. Huang, C. Bao, Y. Yan, N. Ahmed, M. P. J. Lavery, B. Erkmen, S. J. Dolinar, M. Tur, M. Neifeld, M. J. Padgett, R. W. Boyd, J. H. Shapiro, and A. E. Willner, Opt. Lett., **39**, 2845, (2014).
32) S. Zhao, J. Leach, L. Gong, J. Ding, and B. Zheng, Opt. Expr. **20**, 452, (2012).
33) X. Yin, H. Chang, X. Cui, J. X. Ma, Y. J. Wang, G. H. Wu, L. Zhang, and X. Xin, Appl. Opt. **57**, 7644, (2018).
34) N. Sakashita, H. Kishikawa, and N. Goto, Proc. Optics & Communications Taiwan, Int'l Conf., 2018, 2018-FRI-P0201-P005.
35) F. Zhu, S. Huang, W. Shao, J. Zhang, M. Chen, W. Zhang, and J. Zeng, Opt. Commun., **396**, 50, (2017).